In vivo monitoring of magnetically labeled mesenchymal stem cells homing to rabbit hepatic VX2 tumors using magnetic resonance imaging

YONG QIN[1-4*], LISHA ZHUO[5*], JINHUA CAI[1-4], XIAOYA HE[1-4], BO LIU[1-4], CHUAN FENG[1-4] and LIN ZHANG[6]

[1]Department of Radiology, Children's Hospital of Chongqing Medical University; [2]Ministry of Education Key Laboratory of Child Development and Disorders; [3]Key Laboratory of Pediatrics in Chongqing; [4]Chongqing International Science and Technology Cooperation Center for Child Development and Disorders, Chongqing 400014; [5]Outpatient Department, 77100 Troops, Chinese People's Liberation Army, Chongqing 400020; [6]Department of Radiology, Xinan Hospital of Third Military Medical University, Chongqing 400038, P.R. China

Received October 1, 2016; Accepted July 20, 2017

DOI: 10.3892/mmr.2017.7902

Abstract. Although mesenchymal stem cells (MSCs) have been demonstrated to possess a tumor-homing feature, their tropism to liver tumors has not been delineated in a visible manner. The aim of the present study was to evaluate the tumor-homing capacity of MSCs and to investigate the spatial and temporal distributions of MSCs in liver tumors using magnetic resonance imaging (MRI). MSCs were colabeled with superparamagnetic iron oxide (SPIO) particles and 4',6-diamidino-2-phenylindole (DAPI), and then transplanted into rabbits with VX2 liver tumors through intravenous injections. The rabbits were subjected to MRI before and at 3, 7 and 14 days after cell transplantation using a clinical 1.5-T MRI system. Immediately after the MRI examination, histological analyses were performed using fluorescence and Prussian blue staining. At 3 days after injection with labeled MSCs, heterogeneous hypointensity was detected on the MRI images of the tumor. At 7 days after transplantation, the tumor exhibited anisointense MRI signal, whereas a hypointense ring was detected at the border of the tumor. At 14 days after transplantation, the MRI signal recovered the hyperintensity. As demonstrated in the histological analyses, the distribution of the iron particles visualized with Prussian blue staining was consistent with the DAPI-stained bright fluorescent nuclei, and the particles corresponded to the hypointense region on the MR images. Thus, systemically administered MSCs could localize to liver tumors with high specificity and possessed a migration feature with active tumor growth. These results demonstrated that the targeting and distribution of the magnetically labeled stem cells in the tumor could be tracked for 7 days *in vivo* using a clinical 1.5-T MRI scanner.

Correspondence to: Professor Jinhua Cai, Department of Radiology, Children's Hospital of Chongqing Medical University, 136 Zhongshan 2nd Road, Yuzhong, Chongqing 400014, P.R. China
E-mail: cai_jinhua@126.com

*Contributed equally

Abbreviations: MSCs, mesenchymal stem cells; MRI, magnetic resonance imaging; SPIO, superparamagnetic iron oxide; DAPI, 4',6-diamidino-2-phenylindole; HCCs, hepatocellular carcinomas; DMEM, Dulbecco's modified Eagle's medium; FBS, fetal bovine serum; PBS, phosphate-buffered saline; PLL, poly-L-lysine

Key words: liver tumor, magnetic resonance imaging, molecular imaging, mesenchymal stem cells, superparamagnetic iron oxide

Introduction

Therapies for hepatocellular carcinomas (HCCs) remain a global problem. Until now, HCCs have been difficult to treat using traditional methods, including surgery and internal medicine. Gene therapy, a modern molecular therapeutic strategy, has a promising future in the treatment of HCCs (1,2). However, the low targeting specificity and the poor transduction efficiency of the therapeutic gene caused by the lack of tumor selectivity are still the main challenges in the gene therapy field. The use of stem cells as vehicles that effectively carry the therapeutic gene and facilitate tropism to the tumor has attracted substantial interest (3,4).

Bone marrow-derived mesenchymal stem cells (MSCs) differentiate into cells of multiple lineages, including osteocytes, adipocytes, myocytes, neurocytes and hepatocytes (5-9). To date, MSCs have been widely used in tissue engineering and regenerative medicine. As reported in recent studies, MSCs exhibit tropism to liver tumors. These stem cells could be recruited to and specifically target the tumor to participate in the formation of the tumor stroma in response to signals sent from the tumor microenvironment (10,11). This tumor-targeting feature makes MSCs a potential candidate for delivering therapeutic genes in gene therapy strategies. MSCs appear to be more advantageous than other cell types due to their abundance, accessibility and ease of genetic manipulation.

The main issue in cell-based therapeutic strategies is how to monitor the fate and migration of cells after injection. A noninvasive method has been developed to track and quantify the transplanted cells by labeling the cells *in vitro* with superparamagnetic iron oxide (SPIO) nanoparticles, followed by magnetic resonance imaging (MRI) *in vivo* (12-16). Our previous study investigated the feasibility of MRI of stem cells that had been transplanted in an acute injury liver model and observed highly specific tropism of magnetically labeled MSCs to the injured liver tissue that was efficiently monitored using MRI (16). To date, there has been no report concerning the *in vivo* tracking of the tropism of MSCs to liver tumors with MRI. Therefore, the aim of the present study was to evaluate the homing capacity of MSCs to liver tumors and to delineate the spatial and temporal distributions of MSCs in liver tumors after transplantation using a clinical 1.5-T MRI system.

Materials and methods

Animals. New Zealand white rabbits (n=10) were used in this study; 2 were used to harvest MSCs, and 8 were used to establish the tumor model. The animals were provided by the Medical Experimental Animal Center of the Third Military Medical University (Chongqing, China) and were maintained under conventional conditions in the Laboratory Animal Center of Chongqing Medical University (Chongqing, China). All the animal experiments were approved by the Ethics Committee of Chongqing Medical University (Chongqing, China) and were performed in strict accordance with the recommendations in the Guide for the Care and Use of Laboratory Animals of Chongqing Medical University. All surgeries were performed under anesthesia with intraperitoneal sodium pentobarbital (Sinopharm Chemical Reagent Co., Ltd., Shanghai, China) at a dose of 30 mg/kg, and all efforts were made to minimize suffering.

Cell harvest and culture. The MSCs were harvested from the long tubular bones of donor rabbits using Caplan's method (17). Briefly, New Zealand white rabbits (150-200 g) were euthanized by cervical dislocation, and the femurs and tibias were isolated. Bone marrow was flushed out from the long bones with Dulbecco's modified Eagle's medium (DMEM; Sigma-Aldrich; Merck KGaA, Darmstadt, Germany) supplemented with 10% fetal bovine serum (FBS; Sigma-Aldrich; Merck KGaA), antibiotics (50 μg/ml streptomycin and 50 IU penicillin/ml) and heparin (10,000 U/ml; Sigma-Aldrich; Merck KGaA). Subsequently, the bone marrow suspension was centrifuged at 251.78 x g at room temperature for 10 min to isolate the MSC cells. These cells were transferred into a 25-cm^2 plastic flat-bottom flask and cultured with DMEM supplemented with 10% FBS and antibiotics. A total of 24 h later, the MSCs adhered to the flask bottom and formed cell colonies. The non-adherent cells were removed from the culture media by repeated washes with phosphate-buffered saline (PBS, pH 7.4) and a subsequent medium change. After reaching 80-90% confluence, the cells were collected using 0.25% trypsin (Sigma-Aldrich; Merck KGaA) and passaged at a ratio of 1:3. After 3 passages, the cells were harvested for further experiments.

Cell labeling. The MSCs were colabeled with SPIO particles and 4',6-diamidino-2-phenylindole (DAPI; Shanghai Bioengineering Co., Shanghai, China) according to a previously developed protocol (16). Briefly, the SPIO particles (Feridex; 50 μg/ml; Advanced Magnetics, Cambridge, MA, USA) were mixed with the transfection agent poly-L-lysine (PLL; Shanghai Bioengineering Co., Shanghai, China) in culture media to obtain a Feridex-PLL complex (the final concentrations were 25 μg/ml for Feridex and 0.75 μg/ml for PLL). Following this, the culture medium containing the Feridex-PLL complex was supplemented with DAPI at a final concentration of 50 μg/ml. Finally, the culture media containing both the Feridex-PLL complex and DAPI were incubated with the cells at room temperature. After a 24-h staining, the excess Feridex-PLL and DAPI were removed by repeated washes with PBS, and the colabeled MSCs were harvested for the subsequent studies. Prussian blue staining was performed at room temperature for 30 min to assess the magnetic labeling efficiency of the labeled cells using a previously reported protocol (16).

Assessment of cell viability. Cell viability was assessed using the trypan blue dye exclusion method. At day 1 and 1, 2, 3 and 4 weeks after labeling, the cells were exposed to trypan blue dye at room temperature for 5 min. Subsequently, the treated cells were observed using a BH2 light microscope (Olympus Corporation, Tokyo, Japan). The non-labeled cells were treated in the same manner as the control. The ratio of the non-stained, viable cells to the total cells (non-stained, viable cells and the stained, nonviable cells) was calculated and defined as the trypan blue resistance rate. The observer was blinded to the labeling procedures to ensure the accuracy of the test.

Animal model and cell transplantation. Adult New Zealand white rabbits of mixed genders, weighing 3.0-3.5 kg, were used to establish the liver tumor model. The tumor implantation procedures are described below. First, the animals were anesthetized with an intravenous injection of 30 mg/kg body weight sodium pentobarbital (Shanghai Sino-West Pharmaceutical Co., Shanghai, China). Second, a midline laparotomy was performed to expose the liver and a 1-mm^3 VX2 tumor fragment was inserted into the subcapsule of the right-medial lobe of the rabbit liver. Next, the liver capsule was manually compressed for ~2 min, and the abdomen was sutured in two layers. The implanted tumor blocks were allowed to grow in the livers for 1 week to develop into solitary lesions with a diameter of ~1 cm, which were detected using MRI. New Zealand white rabbits with tumors (n=8) were randomly divided into two groups. In the labeled cells group (n=4), rabbits were intravenously injected with 1x10^6 magnetically labeled MSCs resuspended in 1 ml DMEM via the marginal ear vein, and the rabbits in the control group (n=4) received the same quantity of non-labeled MSCs.

In vivo MRI. The rabbits in the experimental and control groups were subjected to MRI immediately before and at 3, 7 and 14 days after cells transplantation. MRI was performed using a clinical 1.5-T MRI system (Signa Excite HD, General Electric, Milwaukee, WI, USA) with a kneel coil. A T2*-weighted gradient-echo sequence was applied to obtain MR images. The imaging acquisition parameters were: TR:TE=25/12, with

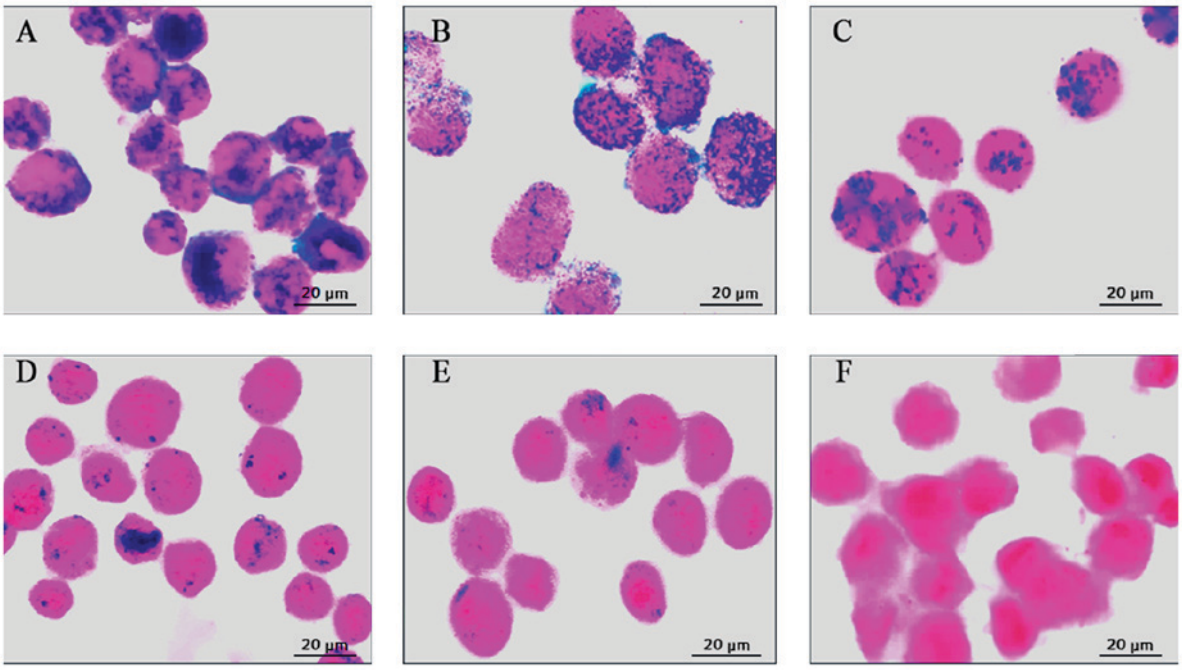

Figure 1. Prussian blue staining of MSCs. (A) Numerous Prussian blue-stained iron particles were detected in the cytoplasm of MSCs at 1 day after magnetic labeling. At (B) 1, (C) 2, and (D) 3 weeks after labeling, the intracellular Prussian blue-stained iron particles faded as the stem cells proliferated. (E) At 4 weeks after labeling, only a few Prussian blue-stained particles were detected. (F) No Prussian blue-stained particles were observed in the unlabeled cells. Scale bar=20 μm. MSCs, mesenchymal stem cells.

a flip angle of 15; field of view: 180x150 mm; matrix size: 256x256; section thickness: 2 mm; number of acquisitions: 2. The signal patterns of the tumors and the adjacent hepatic parenchyma were observed and compared.

Postmortem analysis. Histological analyses were performed immediately after the MRI examination. One experimental rabbit and one control rabbit were sacrificed by an intraperitoneal injection of an overdose of pentobarbital sodium at each time point. By midline laparotomy, the liver tumors were extracted from the abdominal cavities of rabbits. The liver specimens were then prepared by freezing, embedding in paraffin, and sectioning into 5-μm-thick slices. Subsequently, Prussian blue staining (at 4˚C for 30 min) and fluorescent observations were alternatively performed on adjacent slices using our previously described protocol (16). The aim was to identify DAPI and Prussian blue double-positive cells. The kidneys, spleens, lungs, hearts, brains and muscles were also subjected to the same histological analyses to assess the distribution of the cells throughout the rabbits using a BX53 fluorescence microscope (Olympus Corporation).

Statistical analysis. All data are expressed as the mean ± standard deviation, and an independent sample t-test was performed to compare the viability of the labeled and non-labeled cells at various time points. The statistical analyses were performed using SPSS version 18 (IBM Corp., Armonk, NY, USA). $P<0.05$ was considered to indicate a statistically significant difference.

Results

In vitro observations of the labeled MSCs. At 1 day after labeling, numerous Prussian blue-stained iron particles were detected in the cytoplasm of MSCs (Fig. 1A). Thereafter, the intracellular Prussian blue-stained iron particles faded as the cells proliferated (Fig. 1B-D). At 4 weeks after labeling, only a small number of Prussian blue-stained iron particles were observed (Fig. 1E). In contrast, no Prussian blue-stained particles were observed in the unlabeled cells (Fig. 1F).

Cell viability, which is presented as the trypan blue resistance rate, was not significantly different between the labeled and non-labeled MSCs at 1 day and 1, 2, 3 and 4 weeks after labeling (Fig. 2).

In vivo MRI of transplanted MSCs. Prior to injection of the labeled MSCs, the liver tumor exhibited hyperintensity in the T2*-weighted MR images (Fig. 3A). At 3 days after cell injection, MRI showed heterogeneous hypointensity in the tumor, with an unclear demarcation (Fig. 3B). At 7 days after cell injection, the tumor exhibited an isointense MRI signal, whereas a hypointense ring was detected at the border of the tumor (Fig. 3C). At 14 days after injection, the MRI signal recovered the hyperintensity to the level observed prior to the cell transplant (Fig. 3D). In contrast, the control rabbits infused with unlabeled cells did not exhibit any changes in the tumor or liver signals within the 2 weeks of follow-up examinations with MRI (data not shown).

Postmortem analysis. The histological findings, including the Prussian blue staining and fluorescence imaging, primarily revealed labeled MSCs in the liver tumors, rather than the non-tumor liver tissue and other organs. Thus, the MSCs targeted the liver tumor with a high specificity. According to the Prussian blue staining, numerous Prussian blue-stained iron particles were detected throughout the tumor at 3 days after cell injection, compared with a few Prussian blue-stained

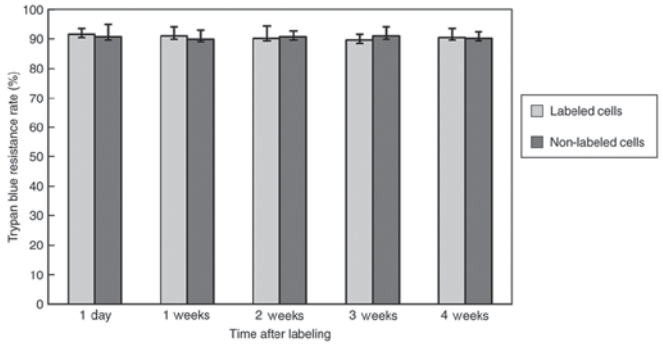

Figure 2. Comparison of cell viability between the labeled and non-labeled cells. Within 4 weeks after cell labeling, no significant difference in trypan blue resistance rate was observed between the labeled and non-labeled cells. Data are presented as the mean ± standard deviation.

iron particles in the adjacent liver tissue (Fig. 4A). However, at 7 days, the Prussian blue-stained iron particles were mainly located at the border of the tumor (Fig. 4B). At 14 days after cell injection, the iron particles remained at the border of the tumor, although the number was obviously decreased (Fig. 4C). This distribution paralleled the distribution observed in the MR images and reflected MSC migration with active tumor growth. Fluorescence microscopy of adjacent sections revealed that the bright, DAPI-stained and fluorescent nuclei matched the distribution of the Prussian blue-stained iron particles (Fig. 5). Therefore, the iron particles remained in the originally labeled cells.

Discussion

As demonstrated in the present study, systemically administered MSCs migrate to hepatic tumors with high specificity, similar to the results observed in our previous study investigating MSC tropism to acutely injured rat livers (16). After homing to the tumor bed, the MSCs scattered throughout the tumor at an early stage and gradually migrated to the border of the tumor at a later stage. The recruitment and distribution of the magnetically labeled MSCs in the liver tumor could be tracked *in vivo* for 1 week using a 1.5-T clinical MRI scanner. These attributes would provide a short-term *in vivo* monitoring strategy for a tumor-targeted therapy.

Homing of MSCs toward experimental tumors has been reported in several animal models, including brain glioma (18), breast cancer (19), lung cancer (20), colon cancer (21) and liver cancer (22). Based on these studies, chemokines released from the tumors are likely to be involved in the mechanism by which MSCs home to tumors. These chemokines would attract stem cells in a manner similar to the mechanism by which the inflammatory factors recruit leukocytes (23). However, the specific chemokines and their contributions to the homing and migration of MSCs have not been well delineated. In contrast to the definite protective effect of leukocytes, the real function of MSCs homing to tumors remains unclear. MSCs were previously demonstrated to promote tumor growth and metastasis by enhancing the tumor neovasculature (24-26), whereas in recent studies, the MSCs did not appreciably contribute to tumor development (27). Furthermore, in other studies, MSCs suppressed tumor progression by modifying and reducing tumor vessels (28,29). These contradictory findings may be attributed to the differences in experimental systems or animal models used. In our study, the distribution of systemically transplanted MSCs in liver tumors varied temporally and spatially with the development of the tumor. At an early stage of tumor growth, the MSCs mainly infiltrated the tumor bed and were scattered throughout the tumor. However, at a later stage, most of the labeled stem cells were detected between the tumor and the surrounding normal parenchyma. Based on these observations, the stem cells migrate in the tumor during tumor growth. Stem cell migration seemed to be associated with the tumor neovasculature, which spread throughout the entire tumor at an early stage and extended to the surrounding region during tumor growth and infringement. In a previous study, Wu *et al* (18) observed the same distribution of transplanted stem cells in gliomas and verified that the stem cells were incorporated into the tumor vessels. Unfortunately, the present study did not investigate the stem cell outcomes because the aim was to visualize the stem cells using MRI; in addition, the stem cells were not visible after 7 days post-transplantation. In this short time period, it is impossible for the stem cells to have been incorporated into the tumor vasculature or differentiated into vascular-related cell lines. A further study should be performed to elucidate the mechanism by which the stem cells migrate in the liver tumor.

Because MSCs have a tumor-homing property and potential applications in tumor gene therapy as a delivery vehicle, the grafted MSCs must be assessed *in vivo* using a noninvasive method. Recent studies have confirmed the feasibility of using MRI to track the stem cells pre-labeled with iron particles prior to transplantation (30-32). In liver cancer, histochemical methods and fluorescence imaging have been used to verify the tumor homing of stem cells (33-36). However, the spatial and temporal distribution of grafted stem cells in the tumor has not been determined. In the present study, homing of the magnetically labeled stem cells to the tumor was observed as a dark signal on the T2*WI images, due to the incorporation of the iron oxide nanoparticles within the cytoplasm. In addition, the dark signal was distributed throughout the tumor at an earlier stage, but it was mainly located at the border of the tumor at a later stage. This pattern of change in the MRI signals paralleled the results of the Prussian blue staining. At 14 days after MSC transplantation, a small number of Prussian blue-positive cells were still observed at the periphery of the liver tumor, whereas no signal change was detected with MRI. Thus, the 1.5-T MRI scanner used in the present study was not sensitive enough to trace the magnetically labeled stem cells due to the reduced number of cells and the dilution of the intracellular iron particles. Therefore, a more effective visualization of the transplanted stem cells at higher magnetic field strengths would be expected.

One problem associated with the SPIO-based *in vivo* MRI tracking of stem cells is determining whether the MRI signal void is generated by the iron particles in the pre-labeled cells. Based on previous studies, the iron particles may be released from dead cells or may be taken up by macrophages, which could lead to misinterpretations of the MRI findings (37,38). In the present study, stem cells were colabeled with SPIO particles and DAPI, and iron was co-localized with the fluorescent marker DAPI in the histological analyses. This result

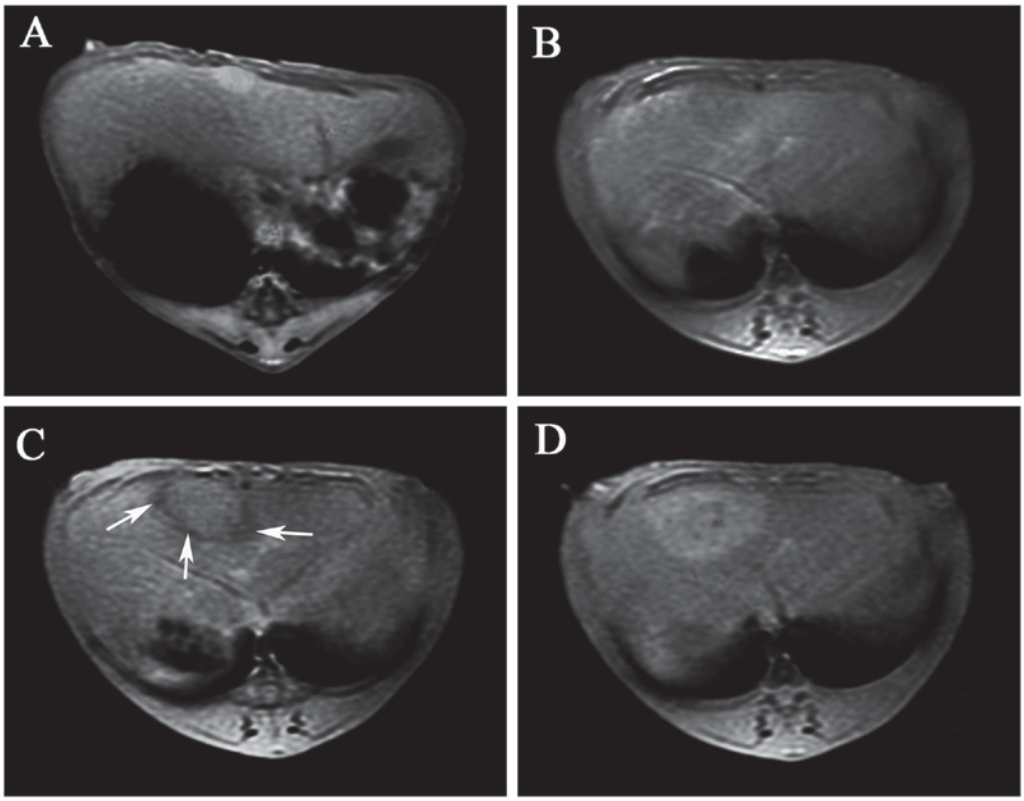

Figure 3. MRI of the liver tumor before and after transplantation of labeled MSCs. (A) The liver tumor was hyperintense on the T2*-weighted image prior to the administration of MSCs. (B) At 3 days after the injection of superparamagnetic iron oxide-labeled MSCs, MR imaging demonstrated heterogeneous hypointensity in the tumor, with an unclear demarcation. (C) At 7 days after transplantation, the MRI signal of the tumor reverted back to isointensity, whereas a hypointense ring was detected at the tumor border (white arrows). (D) At 14 days after transplantation, the hypointense ring disappeared, and the MRI signal recovered to the level observed prior to transplantation. MSCs, mesenchymal stem cells; MRI, magnetic resonance imaging.

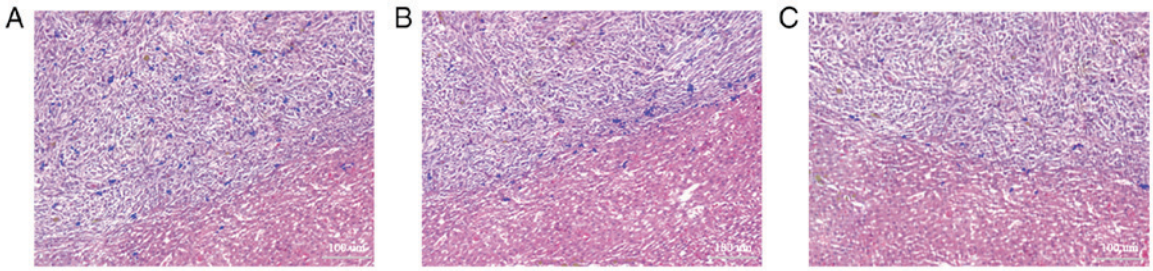

Figure 4. Prussian blue staining of the liver tumor after transplantation of labeled stem cells. (A) At 3 days after cell transplantation, Prussian blue-stained iron particles were primarily distributed throughout the liver tumor, rather than non-tumor liver tissue. (B) At 7 days after cell transplantation, Prussian blue-stained iron particles were mainly located at the tumor border. (C) At 14 days after cell transplantation, Prussian blue-stained iron particles remained at the tumor border, although the number of stained cells was obviously decreased. Scale bar=100 μm.

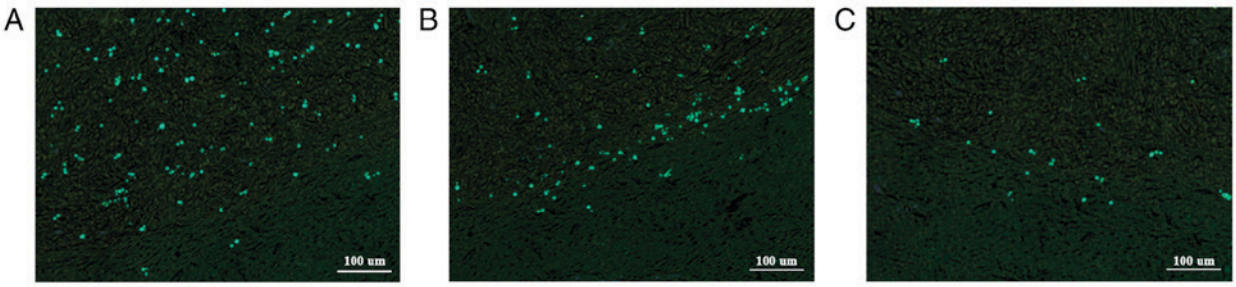

Figure 5. Fluorescence micrographs of the liver tumor after transplantation of labeled stem cells. (A) Numerous DAPI-positive nuclei were distributed throughout the liver tumor at 3 days after stem cell transplantation. (B) The DAPI-positive nuclei were mainly located at the tumor border 7 days after stem cell transplantation. (C) At 14 days after stem cell transplantation, the DAPI-positive nuclei remained at the tumor border, although the number of DAPI-positive cells was obviously decreased. The distribution of the DAPI-stained blue fluorescent nuclei paralleled the distribution of the Prussian blue-stained iron particles. Scale bar=100 μm. DAPI, 4',6-diamidino-2-phenylindole.

excluded the possibility that the MRI signal was generated by the iron released from dead stem cells. On the other hand, both the MRI and histological findings demonstrated varied distribution patterns of cells at the different time points, which is consistent with the migratory feature of stem cells other than of phagocytes. If the released iron was taken up by phagocytes in the tumor, the change in the signal would be persistent. However, in the present study, the change in the MRI signal was not detected at 7 days after cell transplantation, indicating that most of the iron in the stem cells had been cleared from the tumors and was not retained in the phagocytes.

Currently, SPIOs are the most widely used contrast agents for labeling and tracking diverse cells, due to their high relaxivity (39-41). However, long-term tracking of the transplanted cells is not possible using this direct labeling approach due to the continuous reduction of the contrast agent in the cells as they divide (42-44), which is also the main limitation of this study. In the present study, the MRI tracking period was only 1 week, which is insufficient to monitor the fate of the transplanted stem cells. To circumvent this problem, it is urgent that a genetic MRI reporter system be used. Prior to transplantation, the cells are transfected with a constitutively expressed reporter gene and subsequently produce MRI contrast within the cells (45). In such a manner, the transplanted stem cells could be persistently traced *in vivo*.

In conclusion, the present study demonstrated that systemically administered MSCs can migrate to liver tumors with high specificity. The distribution patterns of the stem cells in the tumors indicated that the stem cells possess a migratory property with active tumor growth. These results indicated that the targeting and distribution of the magnetically labeled stem cells in liver tumor can be tracked *in vivo* using a clinical 1.5-T MRI scanner. However, the duration of the MRI tracking is only 1 week because the intracellular iron is diluted as the cells proliferate. Thus, a genetic MRI reporter system must be developed for long-term longitudinal *in vivo* tracking of stem cells used as a therapeutic strategy.

Acknowledgements

This study was supported by a grant from the National Natural Science Foundation of China (81171387). The manuscript has been modified by American Journal Experts editing service.

References

1. Badawy AA, El-Hindawi A, Hammam O, Moussa M, Gabal S and Said N: Impact of epidermal growth factor receptor and transforming growth factor-α on hepatitis C virus-induced hepatocarcinogenesis. APMIS 123: 823-831, 2015.
2. Marquardt JU, Galle PR and Teufel A: Molecular diagnosis and therapy of hepatocellular carcinoma (HCC): An emerging field for advanced technologies. J Hepatol 56: 267-275, 2012.
3. Prieto J, Fernandez-Ruiz V, Kawa MP, Sarobe P and Qian C: Cells as vehicles for therapeutic genes to treat liver diseases. Gene Ther 15: 765-771, 2008.
4. Choi SA, Lee YE, Kwak PA, Lee JY, Kim SS, Lee SJ, Phi JH, Wang KC, Song J, Song SH, *et al*: Clinically applicable human adipose tissue-derived mesenchymal stem cells delivering therapeutic genes to brainstem gliomas. Cancer Gene Ther 22: 302-311, 2015.
5. Heino TJ and Hentunen TA: Differentiation of osteoblasts and osteocytes from mesenchymal stem cells. Curr Stem Cell Res Ther 3: 131-145, 2008.
6. Gou S, Wang C, Liu T, Wu H, Xiong J, Zhou F and Zhao G: Spontaneous differentiation of murine bone marrow-derived mesenchymal stem cells into adipocytes without malignant transformation after long-term culture. Cells Tissues Organs 191: 185-192, 2010.
7. Quevedo HC, Hatzistergos KE, Oskouei BN, Feigenbaum GS, Rodriguez JE, Valdes D, Pattany PM, Zambrano JP, Hu Q, McNiece I, *et al*: Allogeneic mesenchymal stem cells restore cardiac function in chronic ischemic cardiomyopathy via trilineage differentiating capacity. Proc Nat Acad Sci 106: 14022-14027, 2009.
8. Liu Q, Cheng G, Wang Z, Zhan S, Xiong B and Zhao X: Bone marrow-derived mesenchymal stem cells differentiate into nerve-like cells in vitro after transfection with brain-derived neurotrophic factor gene. In Vitro Cell Dev Biol Anim 51: 319-327, 2015.
9. Ke Z, Mao X, Li S, Wang R, Wang L and Zhao G. Dynamic expression characteristics of Notch signal in bone marrow-derived mesenchymal stem cells during the process of differentiation into hepatocytes 45: 95-100, 2013.
10. Abd-Allah SH, Shalaby SM, El-Shal AS, Elkader EA, Hussein S, Emam E, Mazen NF, El Kateb M and Atfy M: Effect of bone marrow-derived mesenchymal stromal cells on hepatoma. Cytotherapy 16: 1197-1206, 2014.
11. Bayo J, Marrodán M, Aquino JB, Silva M, García MG and Mazzolini G: The therapeutic potential of bone marrow-derived mesenchymal stromal cells on hepatocellular carcinoma. Liver International 34: 330-342, 2014.
12. Hua P, Wang YY, Liu LB, Liu JL, Liu JY, Yang YQ and Yang SR: In vivo magnetic resonance imaging tracking of transplanted superparamagnetic iron oxide-labeled bone marrow mesenchymal stem cells in rats with myocardial infarction. Mol Med Rep 11: 113-120, 2015.
13. Markides H, Kehoe O, Morris RH and El Haj AJ: Whole body tracking of superparamagnetic iron oxide nanoparticle-labelled cells-a rheumatoid arthritis mouse model. Stem Cell Res Ther 4: 126, 2013.
14. Jackson JS, Golding JP, Chapon C, Jones WA and Bhakoo KK: Homing of stem cells to sites of inflammatory brain injury after intracerebral and intravenous administration: A longitudinal imaging study. Stem Cell Res Ther 1: 17, 2010.
15. Wei MQ, Wen DD, Wang XY, Huan Y, Yang Y, Xu J, Cheng K and Zheng MW: Experimental study of endothelial progenitor cells labeled with superparamagnetic iron oxide in vitro. Mol Med Rep 11: 3814-3819, 2014.
16. Cai J, Zhang X, Wang X, Li C and Liu G: In vivo MR imaging of magnetically labeled mesenchymal stem cells transplanted into rat liver through hepatic arterial injection. Contrast Media Mol Imaging 3: 61-66, 2008.
17. Wakitani S, Saito T and Caplan AI: Myogenic cells derived from rat bone marrow mesenchymal stem cells exposed to 5-azacytidine. Muscle Nerve 18: 1417-1426, 1995.
18. Wu X, Hu J, Zhou L, Mao Y, Yang B, Gao L, Xie R, Xu F, Zhang D, Liu J and Zhu J: In vivo tracking of superparamagnetic iron oxide nanoparticle-labeled mesenchymal stem cell tropism to malignant gliomas using magnetic resonance imaging. J Neurosurg 108: 320-329, 2008.
19. Zhao D, Najbauer J, Annala AJ, Garcia E, Metz MZ, Gutova M, Polewski MD, Gilchrist M, Glackin CA, Kim SU and Aboody KS: Human neural stem cell tropism to metastatic breast cancer. Stem Cells 30: 314-325, 2012.
20. Xin H, Kanehira M, Mizuguchi H, Hayakawa T, Kikuchi T, Nukiwa T and Saijo Y: Targeted delivery of CX3CL1 to multiple lung tumors by mesenchymal stem cells. Stem Cells 25: 1618-1626, 2007.
21. Yi BR, Park MA, Lee HR, Kang N, Choi KJ, Kim SU and Choi KC: Suppression of the growth of human colorectal cancer cells by therapeutic stem cells expressing cytosine deaminase and interferon-β via their tumor-tropic effect in cellular and xenograft mouse models. Mol Oncol 7: 543-554, 2013.
22. Yan C, Yang M, Li Z, Li S, Hu X, Fan D, Zhang Y, Wang J and Xiong D: Suppression of orthotopically implanted hepatocarcinoma in mice by umbilical cord-derived mesenchymal stem cells with sTRAIL gene expression driven by AFP promoter. Biomaterials 35: 3035-3043, 2014.
23. Fox JM, Chamberlain G, Ashton BA and Middleton J: Recent advances into the understanding of mesenchymal stem cell trafficking. Br J Haematol 137: 491-502, 2007.
24. Zhang T, Lee Y, Rui Y, Cheng T, Jiang X and Li G: Bone marrow-derived mesenchymal stem cells promote growth and angiogenesis of breast and prostate tumors. Stem Cell Res Ther 4: 70, 2013.

25. Suzuki K, Sun R, Origuchi M, Kanehira M, Takahata T, Itoh J, Umezawa A, Kijima H, Fukuda S and Saijo Y: Mesenchymal stromal cells promote tumor growth through the enhancement of neovascularization. Mol Med 17: 579-587, 2011.
26. Hou Y, Ryu CH, Jun JA, Kim SM, Jeong CH and Jeun S-S: IL-8 enhances the angiogenic potential of human bone marrow mesenchymal stem cells by increasing vascular endothelial growth factor. Cell BiolInt 38: 1050-1059, 2014.
27. Usha L, Rao G, Christopherson K and Xu X: Mesenchymal stem cells develop tumor tropism but do not accelerate breast cancer tumorigenesis in a somatic mouse breast cancer model. PLoS One 8: e67895, 2013.
28. Kéramidas M, de Fraipont F, Karageorgis A, Moisan A, Persoons V, Richard MJ, Coll JL and Rome C: The dual effect of mscs on tumour growth and tumour angiogenesis. Stem Cell Res Ther 4: 41, 2013.
29. Gomes C: The dual role of mesenchymal stem cells in tumor progression. Stem Cell Res Ther 4: 42, 2013.
30. Azzabi F, Rottmar M, Jovaisaite V, Rudin M, Sulser T, Boss A and Eberli D: Viability, differentiation capacity, and detectability of super-paramagnetic iron oxide-labeled muscle precursor cells for magnetic-resonance imaging. Tissue Eng Part C Methods 21: 182-191, 2015.
31. Wang Y-X, Xuan S, Port M and Idee J-M: Recent advances in superparamagnetic iron oxide nanoparticles for cellular imaging and targeted therapy research. Curr Pharm Des 19: 6575-6593, 2013.
32. Yang Y, Zhang J, Qian Y, Dong S, Huang H, Boada FE, Fu FH and Wang JH: Superparamagnetic iron oxide is suitable to label tendon stem cells and track them in vivo with MR imaging. Ann Biomed Eng 41: 2109-2119, 2013.
33. Niess H, Bao Q, Conrad C, Zischek C, Notohamiprodjo M, Schwab F, Schwarz B, Huss R, Jauch KW, Nelson PJ and Bruns CJ: Selective targeting of genetically engineered mesenchymal stem cells to tumor stroma microenvironments using tissue-specific suicide gene expression suppresses growth of hepatocellular carcinoma. Ann Surg 254: 767-774, 2011.
34. Gong P, Wang Y, Wang Y, Jin S, Luo H, Zhang J, Bao H and Wang Z: Effect of bone marrow mesenchymal stem cells on hepatocellular carcinoma in microcirculation. Tumor Biol 34: 2161-2168, 2013.
35. Belmar-Lopez C, Mendoza G, Oberg D, Burnet J, Simon C, Cervello I, Iglesias M, Ramirez JC, Lopez-Larrubia P, Quintanilla M and Martin-Duque P: Tissue-derived mesenchymal stromal cells used as vehicles for anti-tumor therapy exert different in vivo effects on migration capacity and tumor growth. BMC Medicine 11: 139, 2013.
36. Klopp AH, Spaeth EL, Dembinski JL, Woodward WA, Munshi A, Meyn RE, Cox JD, Andreeff M and Marini FC: Tumor irradiation increases the recruitment of circulating mesenchymal stem cells into the tumor microenvironment. Cancer Res 67: 11687-11695, 2007.
37. Terrovitis J, Stuber M, Youssef A, Preece S, Leppo M, Kizana E, Schär M, Gerstenblith G, Weiss RG, Marbán E and Abraham MR: Magnetic resonance imaging overestimates ferumoxide-labeled stem cell survival after transplantation in the heart. Circulation 117: 1555-1562, 2008.
38. Amsalem Y, Mardor Y, Feinberg MS, Landa N, Miller L, Daniels D, Ocherashvilli A, Holbova R, Yosef O, Barbash IM and Leor J: Iron-oxide labeling and outcome of transplanted mesenchymal stem cells in the infarcted myocardium. Circulation 116: 38-45, 2007.
39. Cohen ME, Muja N, Fainstein N, Bulte JWM and Ben-Hur T: Conserved fate and function of ferumoxides-labeled neural precursor cells in vitro and in vivo. J Neurosci Res 88: 936-944, 2009.
40. Barczewska M, Wojtkiewicz J, Habich A, Janowski M, Adamiak Z, Holak P, Matyjasik H, Bulte JW, Maksymowicz W and Walczak P: MR monitoring of minimally invasive delivery of mesenchymal stem cells into the porcine intervertebral disc. PLoS One 8: e74658, 2013.
41. England TJ, Bath PMW, Abaei M, Auer D and Jones DRE: Hematopoietic stem cell (CD34+) uptake of superparamagnetic iron oxide is enhanced by but not dependent on a transfection agent. Cytotherapy 15: 384-390, 2013.
42. Lee J-H, Jung MJ, Hwang YH, Lee YJ, Lee S, Lee DY and Shin H: Heparin-coated superparamagnetic iron oxide for in vivo MR imaging of human MSCs. Biomaterials 33: 4861-4871, 2012.
43. Farrell E, Wielopolski P, Pavljasevic P, van Tiel S, Jahr H, Verhaar J, Weinans H, Krestin G, O'Brien FJ, van Osch G and Bernsen M: Effects of iron oxide incorporation for long term cell tracking on MSC differentiation in vitro and in vivo. Biochem Biophys Res Commun 369: 1076-1081, 2008.
44. Arbab AS, Bashaw LA, Miller BR, Jordan EK, Bulte JWM and Frank JA: Intracytoplasmic tagging of cells with ferumoxides and transfection agent for cellular magnetic resonance imaging after cell transplantation: Methods and techniques. Transplantation 76: 1123-1130, 2003.
45. He X, Cai J, Liu B, Zhong Y and Qin Y: Cellular magnetic resonance imaging contrast generated by the ferritin heavy chain genetic reporter under the control of a Tet-On switch. Stem Cell Res Ther 6: 207, 2015.